Volume 14
Number 38
14 October 2022
Pages 13847-14306

Nanoscale

rsc.li/nanoscale

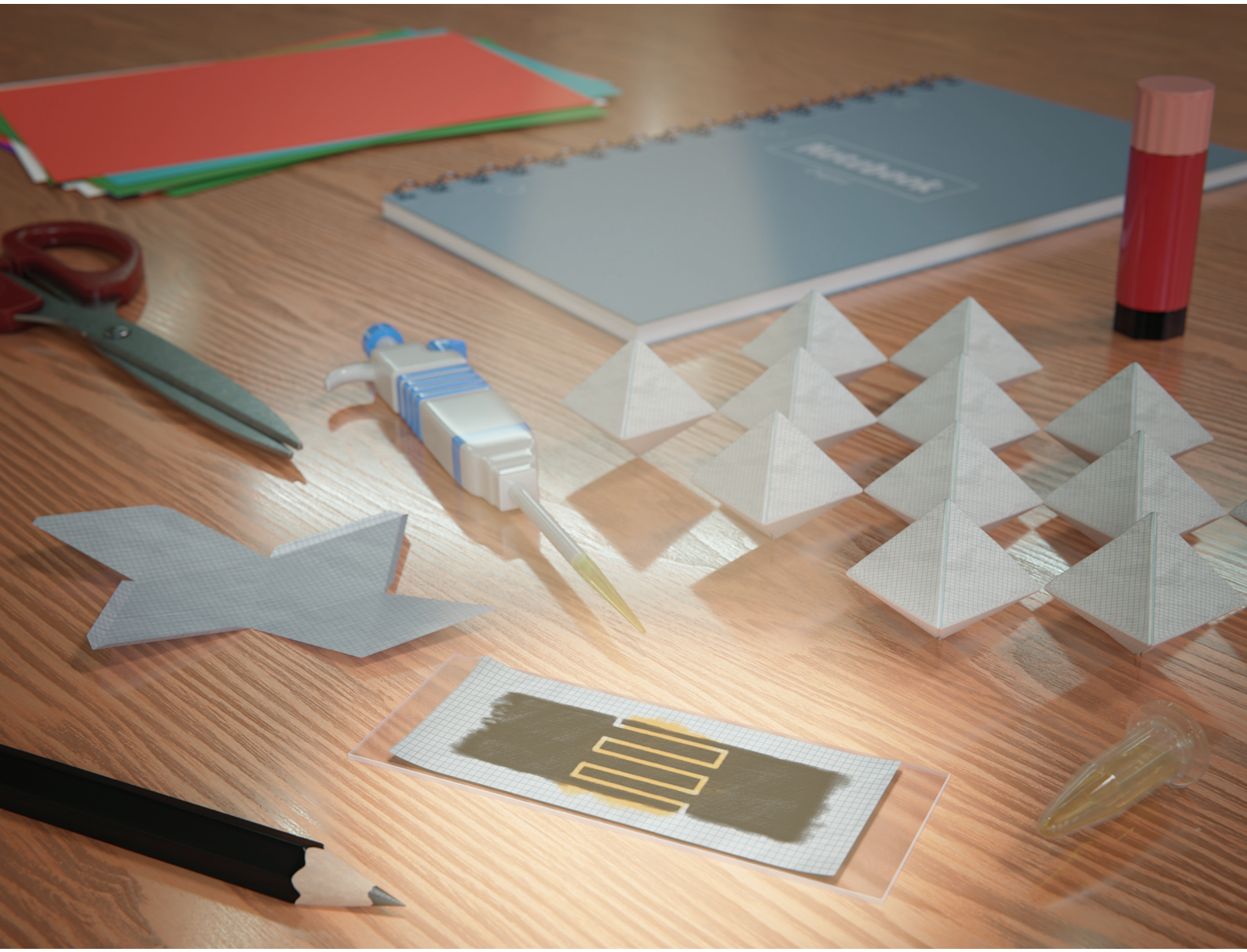

ISSN 2040-3372

ROYAL SOCIETY OF CHEMISTRY

PAPER
Ferry Prins, Andres Castellanos-Gomez *et al.*
Broadband-tunable spectral response of perovskite-on-paper photodetectors using halide mixing

NCNST

Nanoscale

ROYAL SOCIETY OF CHEMISTRY

PAPER

View Article Online
View Journal | View Issue

Cite this: *Nanoscale*, 2022, **14**, 14057

Broadband-tunable spectral response of perovskite-on-paper photodetectors using halide mixing†

Alvaro J. Magdaleno, [a,b] Riccardo Frisenda,[c,d] Ferry Prins *[a,b] and Andres Castellanos-Gomez *[c]

Paper offers a low-cost and widely available substrate for electronics. It possesses alternative characteristics to silicon, as it shows low density and high flexibility, together with biodegradability. Solution processable materials, such as hybrid perovskites, also present light and flexible features, together with a huge tunability of the material composition with varying optical properties. In this study, we combine paper substrates with halide-mixed perovskites for the creation of low-cost and easy-to-prepare perovskite-on-paper photodetectors with a broadband-tunable spectral response. From the bandgap tunability of halide-mixed perovskites we create photodetectors with a cut-off spectral onset that ranges from the NIR to the green region, by increasing the bromide content on $MAPb(I_{1-x}Br_x)_3$ perovskite alloys. The devices show a fast and efficient response. The best performances are observed for pure I and Br perovskite compositions, with a maximum responsivity of ~400 mA W^{-1} on the $MAPbBr_3$ device. This study provides an example of the wide range of possibilities that the combination of solution processable materials with paper substrates offers for the development of low-cost, biodegradable and easy-to-prepare devices.

Received 29th May 2022,
Accepted 31st August 2022

DOI: 10.1039/d2nr02963d

rsc.li/nanoscale

Introduction

Paper has emerged as a promising substrate for electronic applications. The most noticeable characteristics of paper are its strongly reduced costs, biodegradation, low mass density, and high flexibility.[1,2] The last two provide opportunities for creating wearable devices that can adapt to different device shapes.[3] However, the preparation of functional devices on paper remains challenging, as commonly used deposition methods for metals and semiconductors require high temperatures. In this context, the emergence of a wide range of solution processable semiconductors is of particular interest.[4,5] The use of these materials as inks has enabled high-throughput preparation methods such as inkjet printing and roll-to-roll processing.[6,7]

Among the various classes of solution-processable semiconductors, metal–halide perovskites have emerged as a particularly versatile material for light-harvesting[8–31] and light-emitting applications.[32,33] Metal–halide perovskites have the general formula of ABX_3, in which A is a small monovalent cation (*e.g.* methylammonium or Cs), B is a divalent metal (*e.g.* Pb or Sn), and X is a halide (*e.g.* Cl, Br, or I). Using concentrated precursor solutions, metal–halide perovskites readily crystallize into their familiar cubic structure of corner-sharing BX_6 octahedra with interstitial A-site cations. Importantly, by varying the composition, broad and continuous tuning of the optical bandgap can be achieved. In the case of lead-halide perovskites, halide mixing can tune the bandgap across several hundred nanometers across the visible range.[34] Mixed-halide perovskites have been employed extensively to fine-tune the emission wavelength in light-emitting devices[35,36] to maximize the absorptive efficiency in tandem solar cells,[37,38] and to optimize the responsivity (R) in photodetectors.[26,27,29–31]

Indeed, previous studies have demonstrated highly efficient perovskite photodetectors with different spectral responses.[10–19,21–24,26,27,30,31] Recent studies on perovskite-on-paper photodetectors have shown the feasibility of making highly deformable and highly efficient devices. The integration of perovskite photosensitive layers on paper substrates was achieved by dip-coating paper substrates in a perovskite precursor solution, drop-casting the precursor solution on the

[a]*Condensed Matter Physics Center (IFIMAC), Universidad Autónoma de Madrid, 28049 Madrid, Spain. E-mail: ferry.prins@uam.es*
[b]*Departamento de Física de la Materia Condensada, Universidad Autónoma de Madrid, 28049 Madrid, Spain*
[c]*Instituto de Ciencia de Materiales de Madrid (ICMM-CSIC), 28049 Madrid, Spain. E-mail: andres.castellanos@csic.es*
[d]*Department of Physics, Sapienza University of Rome, 00185 Rome, Italy*
† Electronic supplementary information (ESI) available. See DOI: https://doi.org/10.1039/d2nr02963d

paper or spray-coating.[39–43] More specifically, one study has demonstrated the development of a tunable photodetector by mixing different cations in a perovskite structure.[39] Although some variation in the spectral response was achieved using different A-site cations,[39] these strategies do not yet make use of the much wider tunability of the optoelectronic properties of the perovskite composition using halide mixing.

Here, we integrate mixed-halide perovskites on paper substrates to develop perovskite-on-paper photodetectors that provide a broadband-tunable spectral response. The onset of the R of our devices can be shifted from the NIR to the green region by increasing the %Br concentration in the MAPb $(I_{1-x}Br_x)_3$ perovskite. For the development of the devices, we combine the drop-casting of perovskite precursor solutions with all-dry abrasion-induced deposition to print graphite electrodes on the paper.[44] Our results demonstrate the advantages of the use of perovskite semiconductors as inks to achieve tailored optical responses for paper-based electronics.

Results and discussion

Device preparation

As a substrate we chose standard copy paper (instead of more specialized papers) to reduce costs and achieve good biodegradability, which is advantageous with respect to other flexible substrates like plastic-based ones. Among the van der Waals materials, graphite is very attractive for the development of optoelectronic devices because of its lack of bandgap together with the possibility of circuit handwriting.[44] The deposition of graphite for device contacts can be performed by rubbing pure graphite powder (MKN-CG-400, LowerFriction) against the surface of the standard copy paper, as previously described by our group for van der Waals materials.[45,46] In this study, we used a vinyl stencil mask to deposit graphite powder with the desired device layout (see Fig. S1†).

Once the device contacts were defined on the paper substrate (Fig. 1a1), $MAPb(I_{1-x}Br_x)_3$ (x = 0, 0.25, 0.5, 0.75, 1) perovskite solutions were made with a 1.67 M concentration and using anhydrous n,n-dimethylformamide (DMF, Sigma, 227056-1L) as a solvent (the details are listed in the ESI†). The perovskite solutions were deposited by drop-casting 100 μL on the area located between the graphite contacts (see Fig. 1a2–3). Subsequently, the device was dried at 60 °C for 1.5 h in a N_2-filled glovebox (for a more detailed explanation see the ESI†). The resulting devices show a perovskite coating on top of the graphite contacts (see Fig. 1a4). Following this procedure, $MAPb(I_{1-x}Br_x)_3$, x = 0, 0.25, 0.5, 0.75 and 1, perovskites on paper photodetectors were created, showing clear colour variations with varying Br concentrations (see Fig. 1b). The perovskite material is observed on both faces of the paper, meaning that it grew using the paper's porous structure as a scaffold. The copy paper used has a thickness of ~100 μm.

Given the sensitivity of perovskite semiconductors to humidity and oxygen, all devices were measured directly after taking them out of the N_2-filled glovebox anaerobic environment. Devices of different compositions were always measured within one hour without observing clear degradation effects. However, longer exposure to ambient conditions can cause significant performance degradation.

Optical characterization

To confirm the bandgap variations of the different mixed-halide perovskites on paper, we performed optical transmissivity together with photoluminescence (PL) measurements. A clear tuning of the transmission spectrum is observed, as shown in Fig. 1c. The transmission is plotted as 1 − transmittance (1 − T/T_0, where T is the light transmitted by the perovs-

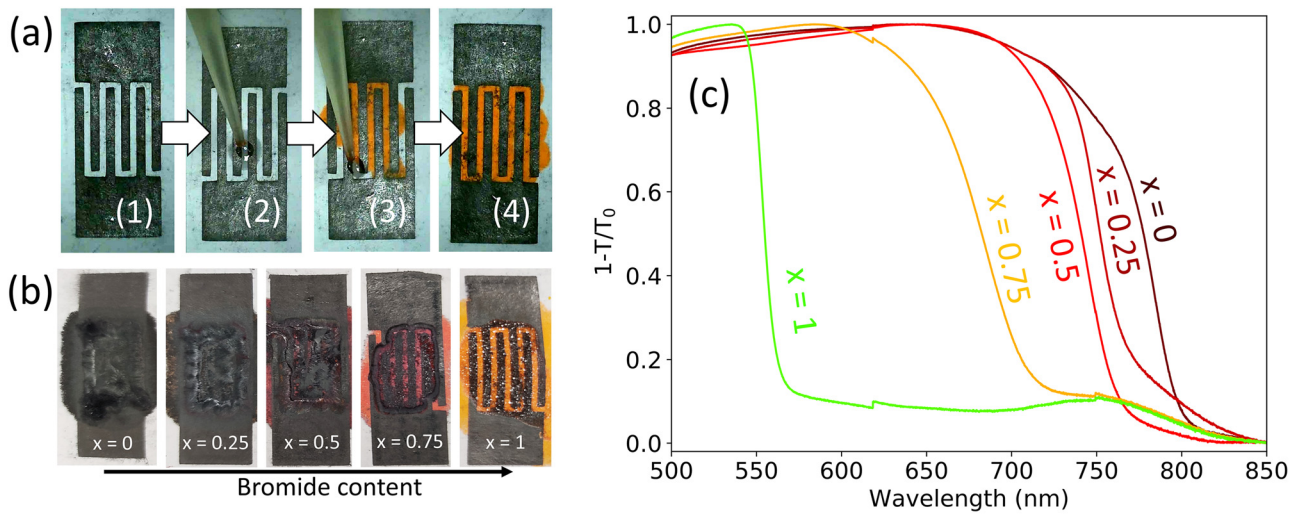

Fig. 1 (a) Device preparation steps: graphite electrodes on paper (1), deposition of perovskite solution (2), covering the complete surface between graphite electrodes (3), and drying perovskite (4). (b) Resulting $MAPb(I_{1-x}Br_x)_3$ devices (increasing %Br from left to right). (c) Resulting transmission (1 − transmittance) of the different perovskite-on-paper films.

kite on paper and T_0 is the light transmitted by a plain paper substrate). For the pure iodide perovskite (x = 0), the transmission edge is located in the NIR region. As the Br concentration (x) is increased, a blue-shifting of the band edge is observed, reaching the onset of transmission in the green region for pure bromide (x = 1). Please note that the transmission spectra of the halide mixtures (x = 0.25, 0.5 and 0.75) show a small red-shift as compared with the PL measurements (see Fig. S2a†). We attribute this shift to light-induced phase segregation originating from the high light intensities that are unavoidable when recording transmission spectra on (only semi-transparent) paper substrates.[47] The PL spectra agree well with the expected bandgap variation when changing the perovskite composition, as can be seen in Fig. S2a.†

Morphological and compositional characterization

To analyse the device morphology and composition along the surface, we employed scanning electron microscopy (SEM) and energy dispersive X-ray spectroscopy (EDX) using a FEI Nova NanoSEM 230. An electron energy of 18 keV was used for EDX spectroscopy.

SEM images of the area between graphite contacts show parts that are covered by a homogeneous and mostly continuous perovskite film on the mm^2 scale, as can be observed in the $MAPbI_3$ sample (Fig. S3a†). As confirmed below in the 'Optoelectronic characterization' section, this device's coverage is enough to obtain a good device functionality. Other parts of the device with a larger density of uncoated regions are also shown where naked paper fibres are observed (see Fig. S3b† for the $MAPbI_3$ device). EDX analysis on the clearest regions of the SEM images is consistent with the presence of the perovskite (see Fig. S3c–e†). There, predominant Pb and I peaks are observed for the x = 0 sample (see Fig. S3e†). For the uncoated regions, EDX analysis shows more prominent peaks at small energies attributed to C and O. Together with the observed Ca peak, this confirms the chemical composition of standard copy paper, which is based on cellulose and calcium carbonate (see Fig. S3f†).

EDX analysis is also consistent with the presence of the corresponding perovskite compositions on the device surface (see Fig. S4†). For x = 0 perovskite films, the EDX spectrum shows peaks at around 2.5 and 4 keV, which are related to Pb and I, respectively. On the other hand, a peak at 1.5 keV characteristic of Br is present in the EDX spectrum of the x = 1 sample instead of the I peaks, while both Br and I peaks are present in the EDX spectrum of the x = 0.5 sample.

Optoelectronic characterization

The performance of the perovskite-on-paper devices as photodetectors was studied by measuring their electrical transport characteristics in a home-built probe station with a source-measure unit (Keithley 2450) in the dark and upon controlled illumination. A light spot of ~71 mm^2 area was used to excite the samples in all the measurements. We used high-power fiber-coupled LED sources (Thorlabs) of different wavelengths (λ_{LED}) connected to a multimode optical fiber (M28L05, Thorlabs) and a collimator (F810SMA-635, Thorlabs) to excite the devices.

First, we analysed the response of our devices to different illumination intensities at fixed wavelengths and with a device bias voltage of 30 V. In Fig. 2a, as *e.g.* $MAPbBr_3$, excited with λ_{LED} = 530 nm, we show the photocurrents generated as a function of time when switching ON and OFF the LED for increased light power (from 1.2 to 54 μW). There is an initial sharp response when the light is turned ON (Fig. 2a, white background) with a subsequent sharp transition to an exponential decay. The transition to different regimes suggests a superposition of different physical effects. The sharp response is typically attributed to the photocurrent generated by the photoconductive effect. Other photogeneration mechanisms like photogating or bolometric effects could be the source of the observed slow response.[48] To compare the device's efficiencies, we calculated the photocurrents by subtracting the background current from the current upon illumination. In addition, we calculated the R of the device using the following equation:

$$R = \frac{I_{ph}}{P} \times \frac{A_{spot}}{A_{sample}}$$

with I_{ph} being the photocurrent, P the illumination intensity, A_{spot} the area of the incident light and A_{sample} the active area of the sample that is under illumination. The photocurrent and R at each light power are plotted (see Fig. 2b, as *e.g.* $MAPbBr_3$, λ_{LED} = 530 nm) to understand the physical origins of the responses of the device. Both variables follow a nonlinear dependence on the excitation light power. In Fig. 2b, we evaluate the power law dependence of the responsivity on the LED power by making a power law fit (R (A W^{-1}) = 0.44P (μW)$^{-0.23}$, see the dashed blue line). This is a common behaviour in both the $MAPbI_3$ and $MAPbBr_3$ perovskite-on-paper photodetectors. The minimum power densities that created device responses were 0.47 ($MAPbI_3$, λ = 660 nm) and 1.66 ($MAPbBr_3$, λ = 530 nm) μW cm^{-2}. These values are close to the smallest minimum operational power densities reported for other perovskite-on-paper devices, which is 0.05 μW cm^{-2} ($MA_{0.6}FA_{0.4}PbI_3$-on-paper, λ = 800 nm, with Cu/Cr/Au electrodes).[39]

Upon illumination of different light sources, the devices show a sub-linear trend, see Fig. 2c (also Fig. S5 and S6† to see the original photocurrents). The sub-linear power dependence suggests that minority charge carrier traps play an important role in photocurrent generation.[48] In fact, with increasingly high-power illumination there is a regime where most of the trap states are already filled in and then the trap-induced photogating effect cannot further contribute to the photocurrent generation.

Second, we characterized the spectral response of our $MAPb(I_{1-x}Br_x)_3$ (x = 0, 0.25, 0.5, 0.75, 1) perovskite-on-paper photodetectors. The photocurrents generated under illumination from 14 different LED sources (Thorlabs, λ_{LED} = 420, 455, 470, 505, 530, 565, 595, 617, 625, 660, 740, 780, 850 and 940 nm) are measured on each photodetector. The illumina-

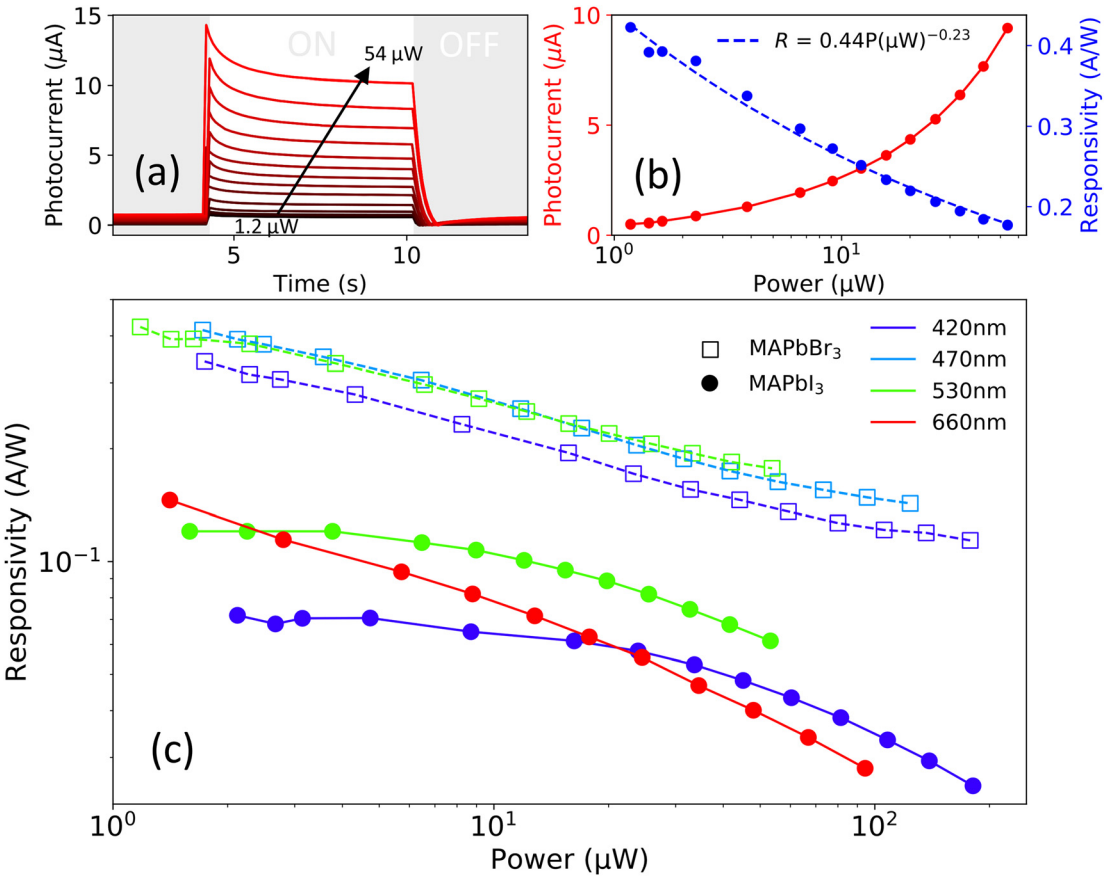

Fig. 2 (a) Power dependence of the photocurrents (*e.g.* $MAPbBr_3$ device, 530 nm LED). (b) Photocurrent (red) and responsivity (blue) dependence on the LED power. The dashed line represents a fitted power law function to the responsivity: R (A W^{-1}) = 0.44P (μW)$^{-0.23}$. (c) Responsivity dependence on the LED power at different excitation wavelengths for $MAPbI_3$ (solid lines) and $MAPbBr_3$ (dashed lines). (a–c) All measurements had a device bias voltage of 30 V.

tion intensity is maintained at 0.365 mW (5 μW mm^{-2}) and the bias voltage of operation of the photodetectors is 1 V. The resulting photocurrents of each device are shown in Fig. S7.†

When the illumination is switched ON (Fig. S7,† white regions), all the measured photocurrents show an initial response whose speed depends on the perovskite compositions (see Fig. S8a and b†). To quantify how fast this response is, we calculated the rise (t_{ON}) and decay (t_{OFF}) times (as the time needed to rise from 10% maximum current to 90%, and from 90% to 10% maximum current, respectively), see Table 1 and Fig. S8c.† For x = 0, 0.75 and 1 the response times of the devices are fast and very similar; both t_{ON} and t_{OFF} are in the range of tenths of seconds. However, the response times of the x = 0.25 and 0.5 devices are slowed down by one (t_{ON} = 5.6 s) and two (t_{ON} = 25 s) orders of magnitude, respectively. We attribute this trend to the different mobilities of the free charges in the perovskite alloys.[49] More importantly though, focusing on the full-width-at-half-maximum of the PL spectra (see Fig. S2b†), a broadening is observed for the x = 0.5 bromide content, which is consistent with earlier reports and can be attributed to disordered perovskite lattices.[49,50] This broadening fits our hypothesis of disorder being the main limitation in the carrier mobility and the performance of the mixed halide photodetectors.[49,51,52] The timescales of the fastest time responses measured within this article are similar to those measured in previous studies, see Table S2.† After the initial response, the photodetectors reach a transition towards a slower regime where the photocurrents saturate (see Fig. S7 and S8a–b†). This transition towards saturation is faster for the x = 0, 0.75 and 1 devices (less than 1 s), while for the x = 0.25 and 0.5 devices it is more gradual (20–60 s, respectively). The x = 0 and 0.75 photodetectors (see Fig. S7 and S7† inset) show a sharp transition towards the slower regime. In these cases, the slower regime is characterized by an exponential decay of the photocurrent towards a constant value. For x = 1,

Table 1 Comparison of the device properties of the different MAPb$(I_{1-x}Br_x)_3$ perovskite-on-paper devices at a bias voltage of 1 V and at a constant incident light power of 0.365 mW (5 μW mm^{-2})

x (%)	R (mA W^{-1})	t_{ON}/t_{OFF} (s)	I_{ON}/I_{OFF}
0	0.43	0.12/0.07	1.60
0.25	0.36	5.61/8.03	1.04
0.5	0.25	25.13/31.0	1.08
0.75	0.05	0.11/0.36	1.13
1	0.57	0.13/0.24	3.26

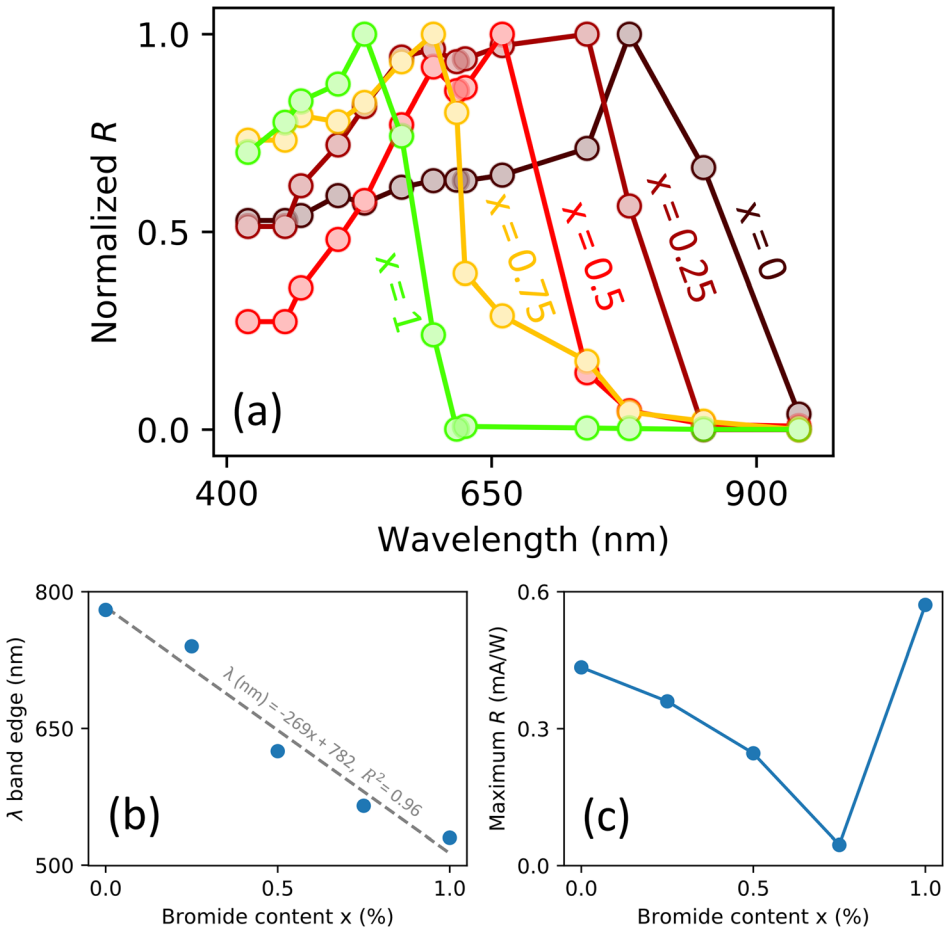

Fig. 3 (a) Normalized device responsivities for each perovskite composition, (b) positions of the onset of the spectral response range of the devices and (c) the maximum responsivity for each device composition. All measurements attributed to this figure were performed at a constant incident light power of 0.365 mW and a voltage of operation of 1 V.

the transition is less sharp but also ends with a similar exponential decay. x = 0.25 and 0.5 photodetectors show a gradual transition until they saturate at a certain photocurrent.

From the photocurrents we can obtain the I_{ON}/I_{OFF} ratio, which is related to the efficiency of the device. In Table 1, we summarize the I_{ON}/I_{OFF} ratios of the different devices at 1 V and at their maximum photocurrents. We observed the highest ratios in the pure I and Br perovskites. However, for the alloys, the bromide content enhances this ratio. The I_{ON}/I_{OFF} ratios achieved by our devices are similar to those achieved in previous studies of perovskite-on-paper devices with graphite contacts, see Table S2.† [41] However, these values are smaller compared with other perovskite-on-paper devices with graphite contacts, probably because a lower incident light power is used in our study, see Table S2.† [42]

The photocurrent and R of the devices at different wavelengths are calculated as described above and shown in Fig. S9.† The normalized R of the devices reveals a modification of the spectral range of response from the NIR to the green region when increasing the bromide content (x, %Br), see Fig. 3a. All devices show a broadband response, as expected from the previously measured transmission range (see Fig. 1c) and other perovskite photodetector studies.[18,19,22,53] It is important to note that the wavelength positions of the maximum R have a linear dependence on x (% Br), see Fig. 3b. This allows the tuning of the onset on the cut-off wavelength position of interest. We also compared the maximum R of each perovskite composition (see Fig. 3c and S9†). They range from 0.0165 to 0.6 mA W^{-1} for the x = 0.75 and 1 devices, respectively. R decreases in the halide mixtures, with the minimum observed at x = 0.75. The decremental device efficiencies present for the halide mixtures are attributed to a disordered electronic structure, as previously suggested for 3D and 2D perovskites, which can lead to electron–hole recombination.[49,54]

Conclusions

In conclusion, we provide a method for the creation of low-cost and easy-to-prepare perovskite-on-paper photodetectors with a broadband-tunable spectral response. Taking advantage

of the bandgap tunability of halide-mixed perovskites, we create perovskite-on-paper photodetectors whose spectral onset ranges from the NIR to the green region, when increasing the bromide content on $MAPb(I_{1-x}Br_x)_3$ alloys. We used straightforward all-dry-abrasion and drop-casting approaches to print the graphite contacts and deposit the perovskite alloys, respectively. This resulted in fast device responses with efficient device performances. The best outputs were achieved on the pure I and Br devices. This study provides a new example of the wide range of properties that solution processable materials together with paper substrates offer for the development of low-cost devices.

Author contributions

A. J. M., A. C. G., R. F. and F. P. performed the experimental work. A. J. M. prepared and measured the devices and carried out the data analysis with assistance from R. F., F. P., and A. C. G. R. F., A. C. G., and A. J. M. carried out the set-up preparation. F. P. and A. C. G. designed and supervised this study.

Conflicts of interest

There are no conflicts to declare.

Acknowledgements

We thank Felix Carrascoso and Wenliang Zhang (ICMM-CSIC) for support with the SEM measurements and the graphite electrode preparation, respectively.

F. P. acknowledges support from the Spanish Ministry for Science, Innovation, and Universities through the state program (PGC2018-097236-A-I00) and the Ramon y Cajal program (RYC-2017-23253). A. C.-G. acknowledges funding from the European Research Council (ERC) under the European Union's Horizon 2020 research and innovation program (grant agreement no. 755655, ERC-StG 2017 project 2D-TOPSENSE), and the Ministry of Science and Innovation (Spain) through the project PID2020-115566RB-I00.

References

1 D. Tobjörk and R. Österbacka, *Adv. Mater.*, 2011, **23**, 1935–1961.
2 A. Russo, B. Y. Ahn, J. J. Adams, E. B. Duoss, J. T. Bernhard and J. A. Lewis, *Adv. Mater.*, 2011, **23**, 3426–3430.
3 S. Cai, X. Xu, W. Yang, J. Chen and X. Fang, *Adv. Mater.*, 2019, **31**, 1808138.
4 F. P. García De Arquer, A. Armin, P. Meredith and E. H. Sargent, *Nat. Rev. Mater.*, 2017, **2**, 16100.
5 Y. Xu and Q. Lin, *Appl. Phys. Rev.*, 2020, **7**, 011315.
6 K. Yan, J. Li, L. Pan and Y. Shi, *APL Mater.*, 2020, **8**, 120705.
7 R. Abbel, Y. Galagan and P. Groen, *Adv. Eng. Mater.*, 2018, **20**, 1701190–1701220.
8 A. Kojima, K. Teshima, Y. Shirai and T. Miyasaka, *J. Am. Chem. Soc.*, 2009, **131**, 6050–6051.
9 J. Burschka, N. Pellet, S. J. Moon, R. Humphry-Baker, P. Gao, M. K. Nazeeruddin and M. Grätzel, *Nature*, 2013, **499**, 316–319.
10 Y. Hou, C. Wu, X. Huang, D. Yang, T. Ye, J. Yoon, R. Sriramdas, K. Wang and P. Priya, *Adv. Funct. Mater.*, 2021, **31**, 2007016–2007029.
11 Y. Fang, Q. Dong, Y. Shao, Y. Yuan and J. Huang, *Nat. Photonics*, 2015, **9**, 679–686.
12 Y. Guo, C. Liu, H. Tanaka and E. Nakamura, *J. Phys. Chem. Lett.*, 2015, **6**, 535–539.
13 G. Maculan, A. D. Sheikh, A. L. Abdelhady, M. I. Saidaminov, M. A. Haque, B. Murali, E. Alarousu, O. F. Mohammed, T. Wu and O. M. Bakr, *J. Phys. Chem. Lett.*, 2015, **6**, 3781–3786.
14 B. R. Sutherland, A. K. Johnston, A. H. Ip, J. Xu, V. Adinolfi, P. Kanjanaboos and E. H. Sargent, *ACS Photonics*, 2015, **2**, 1117–1123.
15 T. Moehl, J. H. Im, Y. H. Lee, K. Domanski, F. Giordano, S. M. Zakeeruddin, M. I. Dar, L. P. Heiniger, M. K. Nazeeruddin, N. G. Park and M. Grätzel, *J. Phys. Chem. Lett.*, 2014, **5**, 3931–3936.
16 R. Dong, Y. Fang, J. Chae, J. Dai, Z. Xiao, Q. Dong, Y. Yuan, A. Centrone, X. C. Zeng and J. Huang, *Adv. Mater.*, 2015, **27**, 1912–1918.
17 F. Tang, Q. Chen, L. Chen, F. Ye, J. Cai and L. Chen, *Appl. Phys. Lett.*, 2016, **109**, 123301.
18 F. Li, C. Ma, H. Wang, W. Hu, W. Yu, A. D. Sheikh and T. Wu, *Nat. Commun.*, 2015, **6**, 8238.
19 L. Zheng, W. Xu, X. Yao, T. Zhu, Y. Yang, L. Liu and X. Gong, *Emergent Mater.*, 2020, **3**, 1–7.
20 M. Liu, M. B. Johnston and H. J. Snaith, *Nature*, 2013, **501**, 395–398.
21 Q. Lin, A. Armin, P. L. Burn and P. Meredith, *Nat. Photonics*, 2015, **9**, 687–694.
22 D. M. Jang, K. Park, D. H. Kim, J. Park, F. Shojaei, H. S. Kang, J. P. Ahn, J. W. Lee and J. K. Song, *Nano Lett.*, 2015, **15**, 5191–5199.
23 M. I. Saidaminov, M. A. Haque, M. Savoie, A. L. Abdelhady, N. Cho, I. Dursun, U. Buttner, E. Alarousu, T. Wu and O. M. Bakr, *Adv. Mater.*, 2016, **28**, 8144–8149.
24 J. Wang, S. Xiao, W. Qian, K. Zhang, J. Yu, X. Xu, G. Wang, S. Zheng and S. Yang, *Adv. Mater.*, 2021, **33**, 2005557.
25 M. A. Green, A. Ho-Baillie and H. J. Snaith, *Nat. Photonics*, 2014, **8**, 506–514.
26 J. Zhou and J. Huang, *Adv. Sci.*, 2018, **5**, 1700256.
27 J. Miao and F. Zhang, *J. Mater. Chem. C*, 2019, **7**, 1741–1791.
28 Y. Dong, Y. Zou, J. Song, X. Song and H. Zeng, *J. Mater. Chem. C*, 2017, **5**, 11369–11394.
29 X. Wang, M. Li, B. Zhang, H. Wang, Y. Zhao and B. Wang, *Org. Electron.*, 2018, **52**, 172–183.

30 S. Qiao, Y. Liu, J. Liu, G. Fu and S. Wang, *ACS Appl. Mater. Interfaces*, 2021, **13**, 34625–34636.
31 Y. Wang, M. L. Gao, J. L. Wu and X. W. Zhang, *Chin. Phys. B*, 2019, **28**, 018502.
32 S. A. Veldhuis, P. P. Boix, N. Yantara, M. Li, T. C. Sum, N. Mathews and S. G. Mhaisalkar, *Adv. Mater.*, 2016, **28**, 6804–6834.
33 Z. K. Tan, R. S. Moghaddam, M. L. Lai, P. Docampo, R. Higler, F. Deschler, M. Price, A. Sadhanala, L. M. Pazos, D. Credgington, F. Hanusch, T. Bein, H. J. Snaith and R. H. Friend, *Nat. Nanotechnol.*, 2014, **9**, 687–692.
34 M. C. Weidman, M. Seitz, S. D. Stranks and W. A. Tisdale, *ACS Nano*, 2016, **10**, 7830–7839.
35 Y. Hassan, J. H. Park, M. L. Crawford, A. Sadhanala, J. Lee, J. C. Sadighian, E. Mosconi, R. Shivanna, E. Radicchi, M. Jeong, C. Yang, H. Choi, S. H. Park, M. H. Song, F. De Angelis, C. Y. Wong, R. H. Friend, B. R. Lee and H. J. Snaith, *Nature*, 2021, **591**, 72–77.
36 Z. Xiao, L. Zhao, N. L. Tran, Y. L. Lin, S. H. Silver, R. A. Kerner, N. Yao, A. Kahn, G. D. Scholes and B. P. Rand, *Nano Lett.*, 2017, **17**, 6863–6869.
37 D. P. McMeekin, G. Sadoughi, W. Rehman, G. E. Eperon, M. Saliba, M. T. Hörantner, A. Haghighirad, N. Sakai, L. Korte, B. Rech, M. B. Johnston, L. M. Herz and H. J. Snaith, *Science*, 2016, **351**, 151–155.
38 M. Jošt, L. Kegelmann, L. Korte and S. Albrecht, *Adv. Energy Mater.*, 2020, **10**, 1904102.
39 A. Maity, A. K. Raychaudhuri and B. Ghosh, *J. Phys. Chem. C*, 2021, **125**, 10646–10652.
40 S. X. Li, X. L. Xu, Y. Yang, Y. S. Xu, Y. Xu and H. Xia, *ACS Appl. Mater. Interfaces*, 2021, **13**, 31919–31927.
41 H. Fang, J. Li, J. Ding, Y. Sun, Q. Li, J. L. Sun, L. Wang and Q. Yan, *ACS Appl. Mater. Interfaces*, 2017, **9**, 10921–10928.
42 F. Cao, D. Yu, X. Li, Y. Zhu, Z. Sun, Y. Shen, Y. Wu, Y. Wei and H. Zeng, *J. Mater. Chem. C*, 2017, **5**, 7441–7445.
43 W. Deng, H. Huang, H. Jin, W. Li, X. Chu, D. Xiong, W. Yan, F. Chun, M. Xie, C. Luo, L. Jin, C. Liu, H. Zhang, W. Deng and W. Yang, *Adv. Opt. Mater.*, 2019, **7**, 1801521.
44 N. Kurra and G. U. Kulkarni, *Lab Chip*, 2013, **13**, 2866–2873.
45 W. Zhang, Q. Zhao, C. Munuera, M. Lee, E. Flores, J. E. F. Rodrigues, J. R. Ares, C. Sanchez, J. Gainza, H. S. J. van der Zant, J. A. Alonso, I. J. Ferrer, T. Wang, R. Frisenda and A. Castellanos-Gomez, *Appl. Mater. Today*, 2021, **23**, 101012.
46 M. Lee, A. Mazaheri, H. S. J. Van Der Zant, R. Frisenda and A. Castellanos-Gomez, *Nanoscale*, 2020, **12**, 22091–22096.
47 S. J. Yoon, M. Kuno and P. V. Kamat, *ACS Energy Lett.*, 2017, **2**, 1507–1514.
48 M. Buscema, J. O. Island, D. J. Groenendijk, S. I. Blanter, G. A. Steele, H. S. J. Van Der Zant and A. Castellanos-Gomez, *Chem. Soc. Rev.*, 2015, **44**, 3691–3718.
49 W. Rehman, R. L. Milot, G. E. Eperon, C. Wehrenfennig, J. L. Boland, H. J. Snaith, M. B. Johnston and L. M. Herz, *Adv. Mater.*, 2015, **27**, 7938–7944.
50 A. Sadhanala, F. Deschler, T. H. Thomas, S. E. Dutton, K. C. Goedel, F. C. Hanusch, M. L. Lai, U. Steiner, T. Bein, P. Docampo, D. Cahen and R. H. Friend, *J. Phys. Chem. Lett.*, 2014, **5**, 2501–2505.
51 W. Rehman, D. P. McMeekin, J. B. Patel, R. L. Milot, M. B. Johnston, H. J. Snaith and L. M. Herz, *Energy Environ. Sci.*, 2017, **10**, 361–369.
52 L. M. Herz, *ACS Energy Lett.*, 2017, **2**, 1539–1548.
53 L. Dou, Y. M. Yang, J. You, Z. Hong, W. H. Chang, G. Li and Y. Yang, *Nat. Commun.*, 2014, **5**, 5404.
54 M. Seitz, M. Meléndez, P. York, D. A. Kurtz, A. J. Magdaleno, N. Alcázar-Cano, A. S. Kshirsagar, M. K. Gangishetty, R. Delgado-Buscalioni, D. N. Congreve and F. Prins, *ACS Energy Lett.*, 2021, 358–365.